

Mid-Infrared Octave-Spanning Supercontinuum and Frequency Comb Generation in a Suspended Germanium-Membrane Ridge Waveguide

Jinhui Yuan, *Member, IEEE, Member, OSA*, Zhe Kang, Feng Li, Xianting Zhang, Xinzhu Sang, *Member, OSA*, Qiang Wu, Binbin Yan, Kuiru Wang, Xian Zhou, *Member, IEEE*, Kangping Zhong, Guiyao Zhou, Chongxiu Yu, Chao Lu, *Fellow, OSA*, Hwa Yaw Tam, *Senior Member, IEEE, Fellow, OSA*, and P. K. A. Wai, *Fellow, IEEE, Fellow, OSA*

I. INTRODUCTION

Abstract—Stable octave-spanning supercontinuum (SC) in the mid-infrared (MIR) region finds extensive applications in spectroscopy, metrology, biochemistry, etc. The absorption of conventional silicon-or silicon oxide-dominated nonlinear media makes SC generation in MIR region technically challenging. In this paper, we propose ultrabroadband MIR-SC generation using a suspended germanium-membrane ridge waveguide. We theoretically showed that when pump pulses centered at 4.8 μm with pulse width at 180 fs and peak power at 800 W are injected into a 4-mm-long proposed ridge waveguide, the SC generated ranges from 1.96–12 μm (about 2.6 octaves), extending deep into the “fingerprint” region. The first-order coherence is calculated to confirm the stability of the generated SC. The performance of the SC-based frequency comb is also investigated by assuming a 100-pulses pump source at a repetition rate of 100 kHz.

This work was supported in part by the National Natural Science Foundation of China (61307109 and 61475023), in part by Beijing Youth Top-notch Talent Support Program (2015000026833ZK08), in part by Natural Science Foundation of Beijing (4152037), in part by the Fund of State Key Laboratory of Information Photonics and Optical Communications (BUPT) China (IPOC2016ZT05), in part by Research Grant Council of the Hong Kong Special Administrative Region China (PolyU152471/16E), and in part by Shenzhen Science and Technology Innovation Commission (JCYJ20160331141313917). J. Yuan and Z. Kang contributed equally to this paper. (*Corresponding author: Zhe Kang and Feng Li.*) J. Yuan, X. Sang, B. Yan, K. Wang, and C. Yu are with the State Key Laboratory of Information Photonics and Optical Communications, Beijing University of Posts and Telecommunications, Beijing, 100876, China. Z. Kang, X. Zhang, X. Zhou, K. Zhong, and C. Lu are with the Photonics Research Centre, Department of Electronic and Information Engineering, The Hong Kong Polytechnic University, Hung Hom, Hong Kong (e-mail: zhe.kang@polyu.edu.hk). F. Li and P. K. A. Wai are with the Photonics Research Centre, Department of Electronic and Information Engineering, The Hong Kong Polytechnic University, Hung Hom, Hong Kong, and also with Hong Kong Polytechnic University, Shenzhen Research Institute, Shenzhen 518057, China (e-mail: enlf@polyu.edu.hk). Q. Wu is with the Department of Physics and Electrical Engineering, Northumbria University, Newcastle upon Tyne NE1 8ST, U.K. G. Zhou is with the Guangdong Provincial Key Laboratory of Nanophotonic Functional Materials and Devices, South China Normal University, Guangzhou 510006, China. H. Y. Tam is with the Photonics Research Centre, Department of Electrical Engineering, The Hong Kong Polytechnic University, Hung Hom, Hong Kong. Color versions of one or more of the figures in this paper are available online

RECENTLY, there have been great interests in mid-infrared (MIR) supercontinuum (SC) generation because of both the technical breakthrough and significant applications in MIR spectroscopy, metrology, biochemical-sensing, etc. [1]–[3]. Two well-known windows important for spectroscopy applications, the functional group (2.5 ~ 7.7 μm) and molecule “fingerprint” regions (7.7 ~ 16.7 μm), lie in the MIR region. The molecular absorption spectra in these regions are derived from the fundamental vibrational frequency of the molecules. Especially within the “fingerprint” region, small change of the molecular structures will lead to significant change in the spectrum. Thus, stable broadband SCs covering these regions provide a useful tool to identify and analyze the molecular characteristics. In addition, temporal coherent and octave-spanning SCs can generate uniform and stable frequency combs, the carrier-envelope phase (CEP) of which can be stabilized by using $f-2f$ self-referencing technique [4], [5]. Such CEP-locked frequency combs will make possible applications, such as optical atom clocks [6] and optical rulers [7].

Group IV photonics materials, i.e. silicon (Si), germanium (Ge), and their derivatives, are suitable for MIR applications [8], [9]. The transparency window of Si in the MIR region ranges from 2.2 to 8.5 μm , while Ge has wider transparency window from 1.5 to 14.3 μm . Propagation loss less than 2 dB/cm can be obtained within the transparency windows [8]. In addition, Si and Ge have much larger linear (about 2.4 ~ 2.7 times) and nonlinear refractive indices (about 2 ~ 3 orders of magnitude) than conventional nonlinear materials (e.g. silica), which allows tighter mode confinement inside the waveguide cores, stronger nonlinear interaction within short waveguide lengths, and lower power threshold of nonlinear interaction [9]–[11]. Moreover, Group IV photonics materials are compatible with the complementary metal oxide semiconductors (CMOS) process. Thus on-chip mass manufacturing of low cost compact Si and Ge based photonic devices is feasible. Conventional silicon-on-insulator (SOI) waveguides have been extensively studied to generate

octave-spanning SCs in the near-infrared (NIR) and shallow MIR regions, e.g. SC with a bandwidth of $2.1\ \mu\text{m}$ spanning $1.5 \sim 3.6\ \mu\text{m}$ [12] and a bandwidth of $1.8\ \mu\text{m}$ spanning $1.5 \sim 3.3\ \mu\text{m}$ [3] in SOI strip waveguides, a bandwidth of $2.25\ \mu\text{m}$ spanning $0.585 \sim 2.833\ \mu\text{m}$ in silicon nitride slot waveguide [9], and a bandwidth of $1.271\ \mu\text{m}$ spanning $0.673 \sim 1.944\ \mu\text{m}$ [13]. However, it is difficult to extend the SCs generated in conventional SOI waveguides deeper into the MIR region because the transparency window of the silicon oxide substrate is limited to $3.6\ \mu\text{m}$. Silicon-on-sapphire (SOS) waveguides have been developed to extend the SC to wavelength $\sim 6\ \mu\text{m}$ [14], which is the upper transparency boundary of sapphire. Further extension of the upper wavelength limit to $\sim 8\ \mu\text{m}$ was obtained by using SOS pillar waveguides with T- and L-like structures to prevent light from leaking into the sapphire substrate [15]. However, since the transparency window of Si is limited to $8.5\ \mu\text{m}$, it is not possible to generate SCs which can significantly cover the “fingerprint” region with conventional Si-based waveguides.

Germanium, as another important branch of Group IV photonics materials, has larger Raman gain coefficient (about 4.5 times) [16], linear (about 1.2 times) [17], [18] and nonlinear refractive indices (about 7 \sim 8 times) [8], [15], [17] than Si. More important, the transparency window of Ge covers most of the “fingerprint” region. SC generation in Si-Ge alloy has been reported, but it is still limited in deep MIR operating at wavelength larger than $8.5\ \mu\text{m}$ owing to the presence of Si [19]. To date, there is only one report on the generation of MIR-SC with crystalline-Ge based waveguide [20]. A $1.34\ \mu\text{m}$ wide SC spanning $3.43 \sim 4.77\ \mu\text{m}$ was obtained using a $2 \times 2\ \mu\text{m}^2$ Ge-on-Si strip waveguide. However, light leakage into the Si substrate at deep MIR region seems inevitable because the refractive index difference between Si and Ge is relatively small, e.g. only 1.2 times at $10\ \mu\text{m}$ [9]. Thus, it would be difficult for this waveguide structure to support efficient SC generation in the “fingerprint” or even deeper MIR region. Finally, we note that chalcogenide glasses, e.g. arsenic sulfide/ selenide, Ge-doped arsenic sulfide/ selenide, etc., also show wide transparency windows that are comparable with Ge. SCs extending deeply into the MIR region using the chalcogenide glass waveguides have been reported [21]–[25]. But, the linear and nonlinear refractive indices of chalcogenide glasses are intrinsically much smaller than that of Ge [9], [26], [27], which would lead to larger cross-sections for mode confinement and stronger energy for the same level nonlinear interaction. Typically, the peak power threshold of several thousand of watts are required to incident into a cross-section of more than a dozen of square microns for deep MIR-SC generation using chalcogenide glass waveguides, thus making the SC generator relatively not compact or power-saving. The requirement of MIR pump source would also be more critical. Therefore, how to take full advantage of Ge while overcoming the limitation on transparency imposed by Si for efficient SC generation with relatively low power consumption extending deeply into the MIR “fingerprint” region and beyond remains challenging.

In this paper, we propose a suspended Ge-membrane ridge waveguide to generate octave-spanning MIR SC that extends deeply into the “fingerprint” region. The primary light-guiding region of the Ge channel is suspended above the Si substrate with

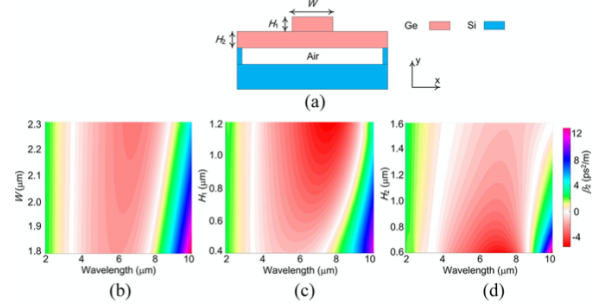


Fig. 1. (a) Cross-section of the proposed suspended Ge-membrane ridge waveguide. Maps of the GVD coefficient (β_2) for the quasi-TE polarization as a function of wavelength when (b) $H_1 \times H_2 = 0.6 \times 0.8\ \mu\text{m}^2$, $W \in 1.8, \dots, 2.3\ \mu\text{m}$, (c) $W \times H_2 = 2.0 \times 0.8\ \mu\text{m}^2$, $H_1 \in 0.4, \dots, 1.2\ \mu\text{m}$, and (d) $W \times H_1 = 2.0 \times 0.8\ \mu\text{m}^2$, $H_2 \in 0.6, \dots, 1.6\ \mu\text{m}$.

an air gap layer so that light cannot leak into the Si substrate even at wavelength of $12\ \mu\text{m}$. Thus, the transparency limitation of Si is eliminated. Meanwhile, since the Ge channel is air-cladded, the proposed waveguides have a much higher refractive index contrast than Ge-on-Si waveguides. The resulting strong mode confinement of the proposed waveguide means a relatively compact structure can be fabricated. The waveguide dimension is carefully designed to obtain the expected dispersion and nonlinear characteristics. The SC and SC-based frequency comb generation in the proposed waveguide are numerically studied with a full model which includes the contributions of high-order nonlinear susceptibility ($\chi^{(5)}$), nonlinear absorption, and Raman scattering.

II. WAVEGUIDE DESIGN

Fig. 1(a) shows the cross-section of the proposed suspended Ge-membrane ridge waveguide. The Ge layer is suspended above the Si substrate with a large air gap. The top of the Ge layer is over-etched to form the membrane ridge structure. The width and height of the ridge core are W and H_1 , respectively, while the height of the membrane layer is H_2 .

The dispersion characteristics of the proposed waveguide for different geometrical parameters are investigated by using the full vector finite element method (FVFEM). Figs. 1(b), (c), and (d) show the maps of the calculated group velocity dispersion (GVD) coefficient (β_2) for the quasi transverse electric (TE) polarization as a function of wavelength when W , H_1 , or H_2 is varied, while the other two parameters are kept constants. The thickness of the air gap is fixed at $2\ \mu\text{m}$ to provide wide enough space between the Ge and Si layers. We observe that in all three cases, two zero dispersion wavelengths (ZDWs) along with a wide anomalous dispersion region can be obtained within the wavelength region of $2 \sim 10\ \mu\text{m}$. We note that the ZDW at the right hand side (longer wavelength) can be red-shifted by increasing either W , H_1 , or H_2 , but the ZDW at the left hand side (shorter wavelength) can be red-shifted by changing H_2 only. Since we want to generate SC which extends deeply into the “fingerprint” region, the ZDW at the left hand side should be located at as long a wavelength as possible so that the pump light could be launched at longer wavelength while remaining close to the ZDW. This can be achieved by carefully selecting

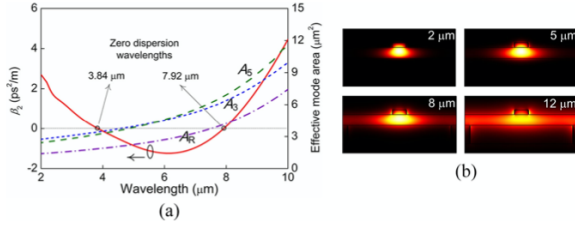


Fig. 2. (a) The calculated GVD coefficient β_2 and effective mode areas A_3 , A_5 , and A_R with respect to $\chi^{(3)}$, $\chi^{(5)}$, and Raman scattering, respectively, as a function of wavelength. (b) Distributions of electronic fields for quasi-TE polarization at 2, 5, 8, and 12 μm , respectively.

H_2 . We also note that when W or H_1 increases, the strength of the GVD coefficient β_2 in the anomalous dispersion region increases, which is not beneficial to the spectral broadening of SC generation. Moreover, increase in W , H_1 , or H_2 will increase the effective mode area, which will weaken the nonlinear interaction for the same waveguide length and power level.

From the above analysis, the geometrical parameters in this work are chosen as $W = 1.8 \mu\text{m}$, $H_1 = 0.5 \mu\text{m}$, and $H_2 = 1.2 \mu\text{m}$, respectively. Fig. 2(a) shows the calculated β_2 for the quasi-TE polarization as a function of wavelength. The wavelength dependence of the material refractive indices of both Ge [9] and Si [9], [28] are considered in the determination of the dispersion characteristic. Two ZDWs located at 3.84 and 7.92 μm are obtained, along with a wide anomalous dispersion region of 4.08 μm . Fig. 2(a) also shows the effective mode areas of A_3 , A_5 , and A_R with respect to the third-order nonlinear susceptibility $\chi^{(3)}$, fifth-order nonlinear susceptibility $\chi^{(5)}$, and Raman scattering, respectively, are given by [20], [29], [30],

$$A_3 = \frac{\frac{Z_0^2}{n_{\text{Ge}}^2} \left| \iint_{D_{\text{total}}} \text{Re} \left\{ \vec{E}(x, y) \times \vec{H}^*(x, y) \right\} \cdot \vec{e}_z dx dy \right|^2}{\iint_{D_{\text{Ge}}} \left| \vec{E}(x, y) \right|^4 dx dy} \quad (1)$$

$$A_5 = \left\{ \frac{\left[\iint_{D_{\text{total}}} \left| \vec{E}(x, y) \right|^2 dx dy \right]^3}{\iint_{D_{\text{Ge}}} \left(\left| \vec{E}(x, y) \right|^2 \right)^3 dx dy} \right\}^{1/2} \quad (2)$$

where $\vec{E}(x, y)$ and $\vec{H}(x, y)$ are the vector electric and magnetic field profiles of the quasi-TE polarization, \vec{e}_z is the unit vector in the positive z -direction, $Z_0 = 377 \Omega$ is the free space wave impedance, n_{Ge} is the material refractive index of Ge, D_{total} and D_{Ge} represent integrals over the whole cross-section and the Ge region, respectively. Fig. 2(b) shows the distributions of electronic fields for quasi-TE polarization at 2, 5, 8, and 12 μm , respectively. We observe that the mode field can hardly leak into the silicon layer even at 12 μm .

III. MODELING

We model the evolution of ultra-short optical pulses propagating inside the proposed waveguide with the generalized nonlinear Schrödinger equation (GNLSE), which includes the contributions of $\chi^{(3)}$, $\chi^{(5)}$, and Raman scattering,

$$\begin{aligned} \frac{\partial \psi}{\partial z} + \frac{(\alpha_l + \sigma N_c)}{2} \psi - i \sum_{k=2}^{\infty} \frac{i^k \beta_k}{k!} \frac{\partial^k \psi}{\partial t^k} \\ = (1 - f_R) \left\{ \sum_{m=1}^2 i \gamma_{2m+1} \left(1 + i \tau_{2m+1} \frac{\partial}{\partial t} \right) |\psi|^{2m} \psi \right\} \\ + i f_R \gamma_R \left(1 + i \tau_R \frac{\partial}{\partial t} \right) \psi \int_{-\infty}^t h_R(t') |\psi(z, t-t')|^2 dt' \\ - \frac{\beta_{3PA}}{3A_5^2} \left(1 + i \tau_{3PA} \frac{\partial}{\partial t} \right) |\psi|^4 \psi + i \frac{2\pi \xi N_c}{\lambda_0} \psi \end{aligned} \quad (4)$$

where $\psi(z, t)$ is the slowly varying envelope of the optical field, t is the time retarded by the phase velocity delay z/v_g induced by the group velocity v_g , α_l is the linear loss coefficient, β_k is the k -th dispersion coefficients, $\gamma_i = \omega_0 n_{(i-1)} / c A_i$, $i = 3, 5, R$ are the real parts of the nonlinear coefficients with respect to $\chi^{(3)}$, $\chi^{(5)}$, and Raman scattering, while $n_{(i-1)}$ are the corresponding nonlinear refractive indices with $n_{(R-1)} = n_2$. β_{3PA} is the three-photon absorption (3PA) coefficient with respect to the imaginary part of $\chi^{(5)}$. The two- and four-photon absorptions are neglected in Eq. (4) because they do not play a dominant role when compared to β_{3PA} within the wavelength region considered [16], [20]. The parameters $\sigma = 5.7942 \times 10^{-22} (\lambda_0 / \lambda_{\text{ref}})^2$ and $\xi = -2.2577 \times 10^{-26} (\lambda_0 / \lambda_{\text{ref}})^2$ are the free carrier coefficients corresponding to the free carrier absorption (FCA) and free carrier dispersion (FCD) effects, where λ_0 is the pump wavelength and λ_{ref} is the reference wavelength of 4 μm [20]. $N_c(z, t)$ is the free carrier density given by,

$$\frac{\partial N_c}{\partial t} = \frac{\beta_{3PA} |\psi|^6}{3\hbar f_0 A_5^3} - \frac{N_c}{\tau_{\text{life}}} \quad (5)$$

where τ_{life} is the effective carrier life, \hbar is the reduced Planck constant, and $f_0 = \omega_0 / 2\pi$ is the center frequency. The time derivative terms in the right hand side of Eq. (4) represent the self-steepening effect and optical shock formation. We take into account the wavelength dependence of the nonlinear refractive indices, the effective mode areas, and the 3PA coefficients by using the full optical shock terms. The parameters of the optical shock terms τ_j , $j = 3, 5, R$, and 3PA, are defined

$$A_R = \frac{\left[\iint_{D_{\text{total}}} \left| \vec{E} \right|^2 dx dy \right]^2}{\iint_{D_{\text{Ge}}} \left(2 \left| \vec{E} \right|^4 + \left| \vec{E} \cdot \vec{E} \right|^2 + \left| \vec{E} \cdot \vec{E}^* \right|^2 - 4 \sum_{i=x,y,z} \left| \vec{E}_i \right|^2 \left| \vec{E}_i \right|^2 \right) dx dy} \quad (3)$$

by [20], [31], [32],

$$\tau_j = \frac{1}{\omega_0} + \frac{1}{n_{(j-1)}(\omega_0)} \frac{dn_{(j-1)}(\omega)}{d\omega} \Big|_{\omega=\omega_0} - \frac{0.5(j-1)}{A_j(\omega_0)} \frac{dA_j(\omega)}{d\omega} \Big|_{\omega=\omega_0} \quad j = 3, 5 \quad (6)$$

$$\tau_R = \frac{1}{\omega_0} + \frac{1}{n_2(\omega_0)} \frac{dn_2(\omega)}{d\omega} \Big|_{\omega=\omega_0} - \frac{1}{A_R(\omega_0)} \frac{dA_R(\omega)}{d\omega} \Big|_{\omega=\omega_0} \quad (7)$$

$$\tau_{3PA} = \frac{1}{\omega_0} + \frac{1}{\beta_{3PA}(\omega_0)} \frac{d\beta_{3PA}(\omega)}{d\omega} \Big|_{\omega=\omega_0} - \frac{2}{A_5(\omega_0)} \frac{dA_5(\omega)}{d\omega} \Big|_{\omega=\omega_0} \quad (8)$$

The integral term in the right hand side of Eq. (4) includes the contribution of the intra-pulse Raman scattering. $h_R(t)$ is the Raman response function which is obtained by fitting the experimental stimulated Raman gain spectrum of Ge in literature [33] with a Lorentzian shape. The corresponding Fourier transform $H_R(\Omega)$ of $h_R(t)$ is given by,

$$H_R(\Omega) = \frac{\Omega_R^2}{\Omega_R^2 - \Omega^2 - 2i\Gamma_R\Omega} \quad (9)$$

where $\Omega_R/2\pi = 9.02$ THz is the Raman shift, $\Gamma_R\pi = 216$ GHz is the bandwidth of Raman gain spectrum. f_R is the fractional contribution of the nuclei to the total nonlinear polarization, which can be calculated from $\text{Im}[H_R(\Omega)] = g_R(\Omega)\lambda_0/4\pi n_2 f_R$ [28]. Here, $g_R(\Omega)$ is Raman gain coefficient of Ge, which can be obtained from [16].

IV. PERFORMANCE AND DISCUSSION

The performance of SC generation inside the proposed waveguide is studied by solving the GNLSE with the split-step Fourier method. A hyperbolic secant shape pulse centered at $4.8 \mu\text{m}$ is used as the pump source. Such MIR optical pulsed sources are feasible from reported works [2], [34], [35]. The linear loss is composed of the intrinsic material loss and the confinement loss of the waveguide. The material loss is chosen as a constant of 2 dB/cm since Ge is transparent within the wavelength regions considered [8], [9]. The confinement loss is calculated by modal analysis using the FVFEM. We find that 99.7% of the total optical energy is confined in the Ge layer when the wavelength is $2 \mu\text{m}$, which corresponds to the confinement loss of only 0.01 dB. However, 96.9% and 76% of the total energy can still be confined in the Ge layer at 4.8 and $12 \mu\text{m}$, respectively, corresponding to the confinement losses of 0.14 and 1.2 dB, respectively. We take into account the wavelength dependence of the confinement loss in our simulation by Taylor expansion of the linear loss coefficient to $\alpha_l = \alpha_l(\omega_0) + \partial\alpha_l/\partial\omega(\omega - \omega_0)$ at the reference frequency ω_0 [32]. The nonlinear refractive indices n_2 and n_4 of Ge are obtained by fitting the results in [9], [16], and [20], which are $2.295 \times 10^{-17} \text{ m}^2/\text{W}$ and $9.47 \times 10^{-32} \text{ m}^4/\text{W}^2$ at $4.8 \mu\text{m}$, respectively. The 3PA coefficient at $4.8 \mu\text{m}$ is found

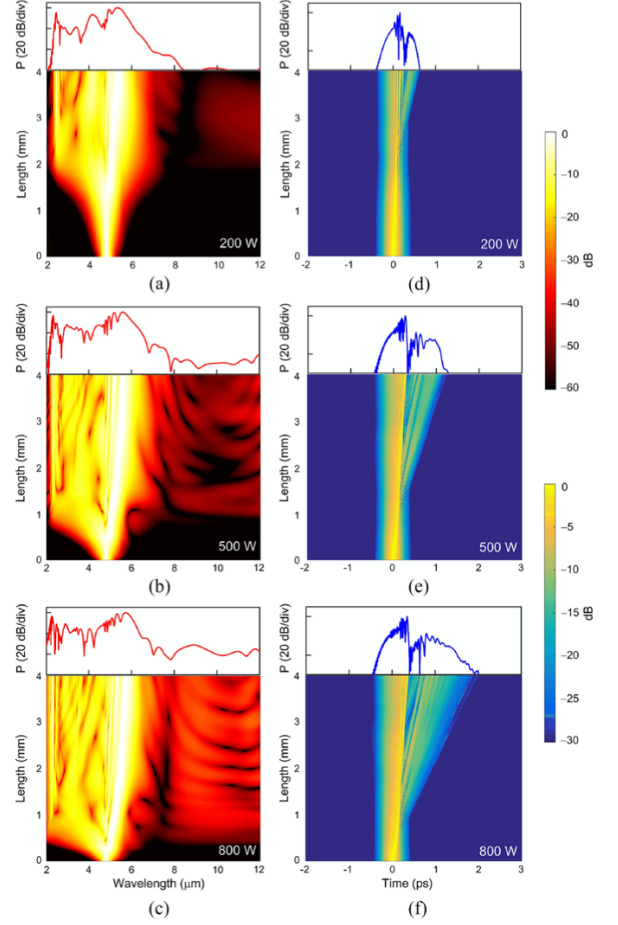


Fig. 3. (a)–(c) The spectral evolution diagrams with the instantaneous spectral profiles, and (d)–(f) the temporal evolution diagrams with the instantaneous temporal profiles, at the output end of the waveguide, when P_0 is 200, 500, and 800 W, respectively.

to be $\beta_{3PA} = 0.005 \text{ cm}^3/\text{GW}^2$, and its wavelength dependence is obtained by fitting the results in [20], [36]. The Raman gain coefficient at $4.8 \mu\text{m}$ is about $g_R = 19 \text{ cm/GW}$, which gives $f_R = 0.076$ [16]. The dispersion parameters are considered up to the eleventh order. Comparing the dispersion effect calculated using the full dispersion coefficients shown in [28] and that using up to the eleventh order dispersion coefficients, the maximum deviation is less than 2.6% in the wavelength region considered. We have repeated some runs of SC simulations using the two different approaches and did not find any significant difference in the final results. The propagation length is fixed at 4 mm. Figs. 3(a)–(c) show the spectral evolutions of the pump pulse with a pulse width (FWHM) of 180 fs inside the 4-mm long proposed waveguide when the input peak power P_0 are 200, 500, and 800 W, respectively. The instantaneous spectral profiles at the output of the waveguide are also illustrated at top of the evolution diagrams. Figs. 3(d)–(f) show the corresponding temporal evolutions and the instantaneous temporal profiles.

For SC generation with the pump source operating in the anomalous dispersion regime, soliton fission and dispersive wave generation make significant contributions to the SC broadening. The soliton fission process can generate several funda-

mental solitons. Each of the resulting solitons will experience intra-pulse Raman scattering induced red-shift and Kerr nonlinear interactions, e.g. self-phase modulation (SPM), cross-phase modulation (XPM), and four-wave mixing (FWM), which would further expand and flatten the SC spectra. Soliton fission is determined by the soliton order $N = (L_D/L_{NL})^{1/2}$ and the soliton fission length $L_{fiss} = L_D/N$. Here, $L_D = T_0^2/|\beta_2|$ and $L_{NL} = 1/(\gamma_3 + \gamma_5 P_0)P_0$ are the dispersion and nonlinear lengths, respectively, and T_0 is the initial pulse width. When $P_0 = 200$ W, $N = 4.7$ and $L_{fiss} \approx 3$ mm are obtained, which agree well with the results shown in Fig. 3(d). Also, we note that dispersive wave around $2.44 \mu\text{m}$ emerges at the propagation length of about 2 mm because of the resonance-matching between the soliton and dispersive wave. The generated dispersive wave further undergoes the Kerr nonlinear interactions, thereby contributes to the SC broadening in the normal dispersion regime of the anti-Stokes side. We use the -40 dB bandwidth to quantify the SC generated, which can be measured using current MIR spectrograph devices [14], [21], [24], [37]. The -40 dB bandwidth obtained in Fig. 3(a) is about $4.6 \mu\text{m}$ covering from 2.28 to $6.88 \mu\text{m}$, which spans almost 1.6 octaves. When P_0 increases to 500 W, the soliton order increases to $N = 7.5$. It is observed that the energy in the normal dispersion regime of the Stokes side is excited because of the contribution of Kerr nonlinear interaction and the dispersive wave generation at the Stokes side. Fig. 3(b) shows that the -40 dB bandwidth is about $5.57 \mu\text{m}$ covering from 2.12 to $7.69 \mu\text{m}$. When the input peak power is further increased to 800 W, much stronger excitation of the spectral intensity are obtained. Fig. 3(c) shows that the -40 dB bandwidth covers from 1.96 to $12 \mu\text{m}$, which spans 2.6 octaves. The gap close to $8 \mu\text{m}$ is mainly caused by the phase perturbation induced by the existence of the ZDW at the Stokes side.

In order to investigate the effects of 3PA and n_4 , i.e. the contributions of the imaginary and real parts of $\chi^{(5)}$ nonlinearity, we study the SC generation with and without the presence of β_{3PA} or n_4 in addition to the $\chi^{(3)}$ nonlinearity and dispersion effects. The pump pulse is assumed to have a FWHM of 80 fs and an input peak power of 500 W. Fig. 4(a) shows the generated SC profiles under different conditions. We observe that the 3PA effect and the corresponding 3PA-induced free carrier effects degrade the broadening of the SC. In contrast, the effect of n_4 shows positive enhancement to the SC broadening. Fig. 4(b) shows the -40 dB bandwidth of the generated SCs as a function of the input peak power under different conditions. We observe that the case with only the effect of n_4 generates the broadest spectrum, which reaches $5.98 \mu\text{m}$ at 500 W. When both n_4 and 3PA are considered, the bandwidth is reduced to $\sim 5.87 \mu\text{m}$ because of the negative contribution of 3PA. The case with only the 3PA effect shows the narrowest bandwidth of $5.46 \mu\text{m}$, which has a bandwidth penalty of $0.52 \mu\text{m}$ compared to that with n_4 only.

Additional loss will be induced in practice because of fabrication defects, e.g. the roughness of the waveguide sidewall and the trapezoidal rather than rectangular cross-sections. For simplicity, we assume the fabrication loss is wavelength independent and simulate the fabrication loss by increasing the material loss

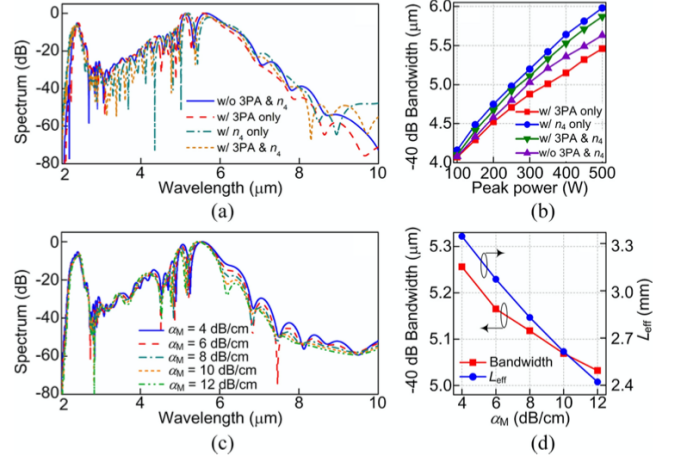


Fig. 4. (a) Spectra under different nonlinear conditions when the input pulse has a FWHM of 80 fs and peak power of 500 W. (b) The -40 dB bandwidth as a function of input peak power under different nonlinear conditions. (c) Spectra under different material loss α_M . (d) The -40 dB bandwidth and the effective propagation length as a function of the material loss α_M .

α_M . Fig. 4(c) shows the SCs generated with all the nonlinear effects considered when α_M is increased from 4 to 12 dB/cm. The parameters used are the same as that in Fig. 4(a). We find that the increase in loss mainly degrades the SC generated at the longer wavelength side. Fig. 4(d) shows the -40 dB bandwidths of the SCs at different α_M . The bandwidth decreases non-linearly with the loss. When α_M is 4 dB/cm, the bandwidth is $5.26 \mu\text{m}$, which is $0.61 \mu\text{m}$ less than that at 2 dB/cm. In comparison, the decrease in bandwidth between $\alpha_M = 10$ and 12 dB/cm is only $0.08 \mu\text{m}$. Fig. 4(d) also shows the effective propagation length defined as $L_{eff} = [1 - \exp(-\alpha_M L)]/\alpha_M$. L_{eff} at $\alpha_M = 12$ dB/cm equals 2.4 mm which is still comparable to the waveguide length 4 mm. Thus the effect of the loss considered on the SC generation is not very significant.

The coherence of the SC is studied by calculating the first-order coherence of the generated spectra, which is given by [32], [38],

$$|g_{1,2}^{(1)}(\lambda)| = \frac{\left| \langle \tilde{\psi}_1^*(\lambda) \tilde{\psi}_2(\lambda) \rangle \right|}{\sqrt{\langle |\tilde{\psi}_1(\lambda)|^2 \rangle \langle |\tilde{\psi}_2(\lambda)|^2 \rangle}} \quad (10)$$

where $\tilde{\psi}(\lambda)$ is the spectral amplitude of the generated SC with random noise seeds. The angular brackets represent ensemble average over the adjacent pairs of SC spectra generated from a large number of simulations. The additive random noise is given by $n = \eta \hat{N} \exp(i2\pi \hat{U})$. Here, \hat{N} is a normally distributed random variable with mean 0 and standard deviation 1 , \hat{U} is a uniformly distributed random variable between 0 and 1 , and η is the noise factor denoting the amplitude of the noise relative to the pulse amplitude. The coherence is calculated for different FWHMs of the pump pulse, i.e. 80 , 200 , and 320 fs, but the same peak power of 800 W and waveguide length of 4 mm. The 100 shot-to-shot spectrum pairs are used for the estimation.

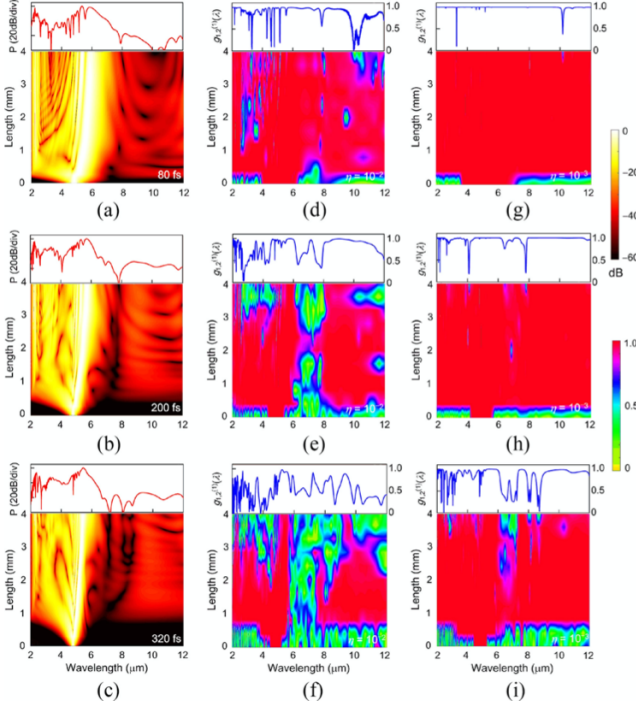


Fig. 5. (a)–(c) show the spectral evolution diagrams along with the instantaneous spectral profiles at the output end of the waveguide when the FWHM of the pulse is 80, 200, and 320 fs, respectively. The corresponding coherence evolution diagrams and the instantaneous coherence profiles are given at different noise factors, (d)–(f) $\eta = 10^{-2}$, and (g)–(i) $\eta = 10^{-3}$, respectively.

Fig. 5 shows the spectral evolution diagrams along with their instantaneous spectral profiles at the output end of the waveguide (Figs. 5(a)–(c)), and the corresponding coherence evolution and instantaneous coherence profile at $\eta = 10^{-2}$ (Figs. 5(d)–(f)) and $\eta = 10^{-3}$ (Figs. 5(g)–(i)) when the FWHM of the pump pulses are 80, 200, and 320 fs, respectively. We observe that the SC spectra are significantly broadened when the pulse width is increased because of the increase in the soliton order N as a result of the increase in the dispersion length L_D . Also, the energy of the pump is effectively increased so that more solitons can be red-shifted. The spectral valley beyond $8 \mu\text{m}$ in Fig. 5(a) is filled up in Fig. 5(b). On the other hand, the spectral gaps in Fig. 5(b) are further excited when the FWHM is increased to 320 fs, as shown in Fig. 5(c). In contrast, the coherence exhibits an almost completely opposite trend. As shown in Figs. 5(d)–(f), which are obtained at the same noise factor $\eta = 10^{-2}$, the coherence degrades obviously when the pulse width is increased. It is because an optical pulse with a larger temporal pulse width generally has a smaller spectral bandwidth. Thus, the average noise intensity covering the bandwidth considered is increased compared to the cases with shorter pulse widths, which leads to more severe spectral instability. Similar phenomena are observed in Figs. 5(g)–(i), where the noise factor is $\eta = 10^{-3}$. As expected, the coherence performances at $\eta = 10^{-3}$ are all better than the corresponding ones at $\eta = 10^{-2}$. For instance, the coherence shown in Fig. 5(g) is close to unity within $2 \sim 12 \mu\text{m}$ except several isolated points of degradation. The points of degradation in general occur at the spectral regime with large

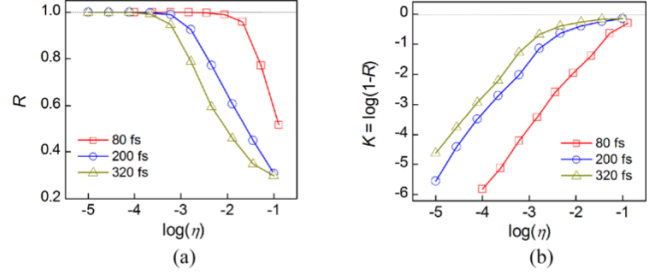


Fig. 6. (a) The weighted degree R and (b) $K = \log(1 - R)$ as a function of $\log(\eta)$ at 80, 200, and 320 fs, respectively.

extinction ratio, where the phases of the spectra change severely. Fig. 5(h) shows that the coherence is close to unity within $3.1 \sim 3.8$, $4.3 \sim 6.2$, and $7.9 \sim 11.6 \mu\text{m}$ at the FWHM of 200 fs. The last wavelength region locates in the “fingerprint” region with a bandwidth of $3.7 \mu\text{m}$. Fig. 5(i) shows that when the FWHM is increased to 320 fs, the coherence is smaller than unity in most of the wavelength regions even at $\eta = 10^{-3}$. Therefore, there is a tradeoff between the degree of broadening and coherence of the generated SC when choosing the pump sources. In addition, the selection of waveguide length also induces similar tradeoff. High degree of coherence generally occurs when the waveguide length just passes the soliton fission length. Additional waveguide length could lead to increase in the spectral bandwidth at the expense of coherence.

The weighted degree of coherence is used to quantitatively estimate the averaged coherence within the whole spectral range of the SCs generated, which is given by [38], [39],

$$R = \frac{\int_0^\infty |g_{1,2}^{(1)}(\lambda)| \bar{P}(\lambda) d\lambda}{\int_0^\infty \bar{P}(\lambda) d\lambda} \quad (11)$$

where $\bar{P}(\lambda) = \langle |\tilde{\psi}(\lambda)|^2 \rangle$ is the ensemble average of the spectra obtained with different noise seeds. Fig. 6(a) shows the calculated R as a function of $\log(\eta)$ at pump pulse widths of 80, 200, and 320 fs, respectively. For the 320 fs pump pulse, R is close to unity until the $\log(\eta)$ reaches -3.7 , and quickly degrades to about 0.3 when $\log(\eta)$ is increased to -1 . In comparison, the 200 fs pump pulse shows a slower degradation rate. When the $\log(\eta)$ is -3 , the R value of the 200 fs pump pulse is as large as 0.97. The 80 fs pump pulse shows a better noise tolerance, its R value remains unity until $\log(\eta) = -2.3$. To clearly show the values that are close to unity in Fig. 6(a), we plot $K = \log(1 - R)$ in Fig. 6(b). The $\log(\eta)$ penalty between 80 and 320 fs pump pulses increases when $\log(\eta)$ decreases and reaches up to 1.6 at $K = -4$.

Fig. 7(a) shows the SC-based frequency comb generated in the proposed waveguide by assuming a pump pulse train with FWHM of 180 fs and peak power of 800 W. The pump pulse train includes 100 pulses with a repetition rate of 100 kHz. In order to clearly show the comb structure, the zoom-in view of two randomly chosen spectral regions locating at A ($51.7 \text{ THz}/5.8 \mu\text{m}$) and B ($29.8 \text{ THz}/10.1 \mu\text{m}$) are shown with a sampling bandwidth of 500 kHz in Figs. 7(b) and (c), respectively. The comb line structure can be clearly seen in both of the zoom-in view

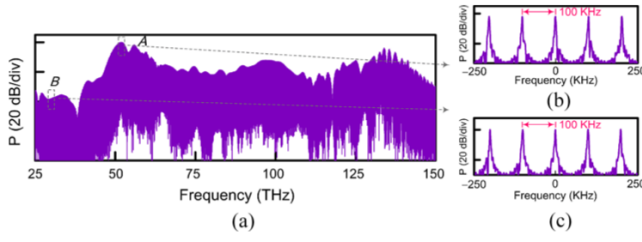


Fig. 7. (a) The SC-based frequency comb obtained with 100 input pulses with repetition rate of 100 kHz. (b) and (c) show the zoom-in view at points A and B marked in (a) with a sampling bandwidth of 500 kHz.

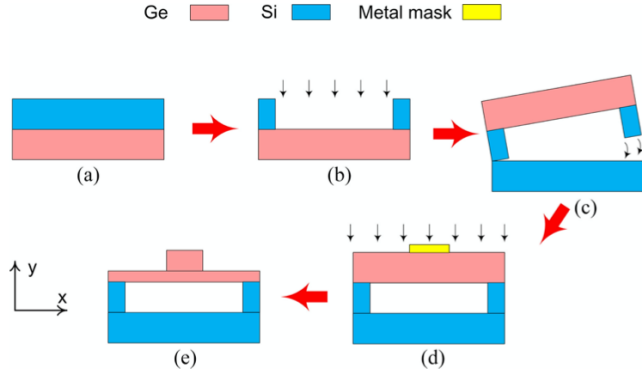


Fig. 8. A possible fabrication process flow: (a) deposition of Ge on Si substrate and inversion, (b) formation of the suspended air trench, (c) Si hydrophobic bonding, (d) waveguide definition with metal mask and etching, and (e) final waveguide structure.

with a frequency interval of 100 kHz. The extinction ratios of the comb lines are found to be not less than 30 dB, which are estimated by the amplitude difference between the peaks and bottoms of each individual comb line.

Figs. 8(a)–(e) show a possible fabrication process of the designed waveguide. First, the Ge layer is grown on a Si substrate by using atmospheric chemical vapor deposition [40]. The formed die is then inverted carefully (Fig. 8(a)). Traditional optical lithography with plasma reactive-ion dry etching is used to form the suspended trench (Fig. 8(b)). The etched die is directly bonded onto the Si wafer by using the hydrophobic bonding techniques (Fig. 8(c)). Detailed bonding process can be found in literature [41]. Finally, a metal mask, which is patterned by i-line lithography and lift-off, is used to define the ridge structure [42]. The over-etching of the Ge layer is accomplished by a $\text{CF}_4:\text{O}_2$ plasma etching, and the metal mask is removed by hydrofluoric acid dip (Fig. 8(d)).

V. CONCLUSION

In summary, we propose a stable octave-spanning MIR-SC and SC-based frequency comb generation using a suspended Ge-membrane ridge waveguide. The generated SC can extend deeply into the application-rich “fingerprint” region, which is hard to be achieved with conventional silicon- or silicon oxide-dominated waveguides. Fabrication of the proposed waveguide is CMOS compatible so that future applications with on-chip mass manufacturing and interconnection are feasible. The per-

formances of the SCs are studied at different pump peak powers and pulse widths. When 180 fs pulses are used to pump at $4.8 \mu\text{m}$ with 800 W peak power, the generated SC in 4 mm of the proposed waveguide can cover $1.96 \sim 12 \mu\text{m}$ in the MIR regions, which spans 2.6 times of an octave. The coherence of the SCs is also investigated at different pulse width by calculating the first-order coherence with 100 shot-to-shot spectrum pairs perturbed by random noise. It is found that the coherence remains unity in most of the spectral regions, including the covered “fingerprint” region, even at pulse width of 200 fs when the noise factor is 10^{-3} . In addition, SC-based frequency combs are achieved by assuming a pump pulse train containing 100 pulses at a repetition rate of 100 kHz. The comb line structure can be clearly seen in zoom-in view randomly chosen in the spectra. The frequency interval of the comb lines is 100 kHz and the extinction ratios of all the individual comb lines are not less than 30 dB. Thus, the proposed SC-based frequency comb is suitable for high-precision applications. The proposed waveguide structure paves the road for the exploration of on-chip MIR-SC generation deep into the “fingerprint” region, which would be of interest to applications such as spectroscopy, metrology, biochemistry, etc.

REFERENCES

- [1] A. Schliesser, N. Picqué, and T. W. Hänsch, “Mid-infrared frequency combs,” *Nature Photon.*, vol. 6, pp. 440–449, Jun. 2012.
- [2] C. R. Petersen *et al.*, “Mid-infrared supercontinuum covering the 1.4–13.3 μm molecular fingerprint region using ultra-high NA chalcogenide step-index fibre,” *Nature Photon.*, vol. 8, pp. 830–834, Mar. 2014.
- [3] B. Kuyken *et al.*, “An octave-spanning mid-infrared frequency comb generated in a silicon nanophotonic wire waveguide,” *Nature Commun.*, vol. 6, Feb. 2015, Art. no. 6310.
- [4] D. J. Jones *et al.*, “Carrier-envelope phase control of femtosecond mode-locked lasers and direct optical frequency synthesis,” *Sci.*, vol. 288, pp. 635–639, Apr. 2000.
- [5] A. Ruehl *et al.*, “Ultrabroadband coherent supercontinuum frequency comb,” *Phys. Rev. A*, vol. 84, no. 1, Jul. 2011, Art. no. 011806(R).
- [6] T. Udem, R. Holzwarth, and T. W. Hänsch, “Optical frequency metrology,” *Nature*, vol. 416, pp. 233–237, Mar. 2002.
- [7] J. N. Eckstein, A. I. Ferguson, and T. W. Hänsch, “High-resolution two-photon spectroscopy with picosecond light pulses,” *Phys. Rev. Lett.*, vol. 40, no. 13, pp. 847–850, Mar. 1978.
- [8] R. Soref, “Mid-infrared photonics in silicon and germanium,” *Nature Photon.*, vol. 4, pp. 495–497, Aug. 2010.
- [9] L. Zhang, A. M. Agarwal, L. C. Kimerling, and J. Michel, “Nonlinear Group IV photonics based on silicon and germanium: from near-infrared to mid-infrared,” *Nanophoton.*, vol. 3, no. 4–5, pp. 247–268, Jan. 2014.
- [10] X. Gai *et al.*, “Nonlinear absorption and refraction in crystalline silicon in the mid-infrared,” *Laser Photon. Rev.*, vol. 7, no. 6, pp. 1054–1064, Oct. 2013.
- [11] H. K. Tsang and Y. Liu, “Nonlinear optical properties of silicon waveguides,” *Semicond. Sci. Technol.*, vol. 23, no. 6, May 2008, Art. no. 064007.
- [12] R. K. W. Lau, M. R. E. Lamont, A. G. Griffith, Y. Okawachi, M. Lipson, and A. L. Gaeta, “Octave-spanning mid-infrared supercontinuum generation in silicon nanowaveguides,” *Opt. Lett.*, vol. 39, no. 15, pp. 4518–4521, Aug. 2014.
- [13] A. R. Johnson *et al.*, “Octave-spanning coherent supercontinuum generation in a silicon nitride waveguide,” *Opt. Lett.*, vol. 40, no. 21, pp. 5117–5120, Nov. 2015.
- [14] N. Singh *et al.*, “Mid-infrared supercontinuum generation from 2 to 6 μm in a silicon nanowire,” *Optica*, vol. 2, no. 9, pp. 797–802, Sep. 2015.
- [15] N. Singh, D. D. Hudson, and B. J. Eggleton, “Silicon-on-sapphire pillar waveguides for Mid-IR supercontinuum generation,” *Opt. Express*, vol. 23, no. 13, pp. 17345–17354, Jun. 2015.
- [16] N. K. Hon, R. Soref, and B. Jalali, “The third-order nonlinear optical coefficients of Si, Ge, and Si1-xGex in the midwave and longwave infrared,” *J. Appl. Phys.*, vol. 110, no. 1, 2011, Art. no. 011301.

- [17] N. P. Barne and M. S. Piltch, "Temperature-dependent Sellmeier coefficients and nonlinear optics average power limit for germanium," *J. Opt. Soc. Amer.*, vol. 69, no. 1, pp. 178–180, Jan. 1979.
- [18] F. D. Leonardis, B. Troia, and V. M. N. Passaro, "Mid-IR optical and nonlinear properties of germanium on silicon optical waveguides," *J. Lightw. Technol.*, vol. 32, no. 22, pp. 3747–3757, Nov. 2014.
- [19] M. A. Ettabib *et al.*, "Broadband telecom to mid-infrared supercontinuum generation in a dispersion engineered silicon germanium waveguide," *Opt. Lett.*, vol. 40, no. 17, pp. 4118–4121, Sep. 2015.
- [20] F. D. Leonardis, B. Troia, R. A. Soref, and V. M. N. Passaro, "Modelling of supercontinuum generation in the germanium-on-silicon waveguided platform," *J. Lightw. Technol.*, vol. 33, no. 21, pp. 4437–4444, Nov. 2015.
- [21] Y. Yu *et al.*, "A broadband, quasi-continuous, mid-infrared supercontinuum generated in a chalcogenide glass waveguide," *Laser Photon. Rev.*, vol. 8, no. 5, pp. 792–798, May 2014.
- [22] Y. Yu *et al.*, "Mid-infrared supercontinuum generation in chalcogenides," *Opt. Mater. Express*, vol. 3, no. 8, pp. 1075–1086, Aug. 2013.
- [23] F. Théberge, N. Thiré, and J. F. Daigle, "Multioctave infrared supercontinuum generation in large-core As_2S_3 fibers," *Opt. Lett.*, vol. 39, no. 22, pp. 6474–6477, Nov. 2014.
- [24] Y. Yu *et al.*, "1.8–10 μm mid-infrared supercontinuum generated in a step-index chalcogenide fiber using low peak pump power," *Opt. Lett.*, vol. 40, no. 6, pp. 1081–1084, Mar. 2015.
- [25] M. R. Karim, B. M. A. Rahman, and G. P. Agrawal, "Mid-infrared supercontinuum generation using dispersion-engineered $\text{Ge}_{11.5}\text{As}_{24}\text{Se}_{64.5}$ chalcogenide channel waveguide," *Opt. Express*, vol. 23, no. 5, pp. 6903–6914, Mar. 2015.
- [26] B. J. Eggleton, B. L. Davies, and K. Richardson, "Chalcogenide photonics," *Nature Photon.*, vol. 5, pp. 141–148, Feb. 2011.
- [27] A. B. Salem, R. Cherif, and M. Zghal, "Soliton-self compression in highly nonlinear chalcogenide photonic nanowires with ultralow pulse energy," *Opt. Express*, vol. 19, no. 21, pp. 19955–19966, Oct. 2011.
- [28] L. H. Yin, Q. Lin, and G. P. Agrawal, "Soliton fission and supercontinuum generation in silicon waveguides," *Opt. Lett.*, vol. 32, no. 4, pp. 391–393, Feb. 2007.
- [29] Z. Kang *et al.*, "CMOS-compatible 2-bit optical spectral quantization scheme using a silicon-nanocrystal-based horizontal slot waveguide," *Sci. Rep.*, vol. 4, Nov. 2014, Art. no. 7177.
- [30] F. D. Leonardis, B. Troia, and V. M. N. Passaro, "Design rules for Raman lasers based on SOI racetrack resonators," *IEEE Photon. J.*, vol. 5, no. 6, Dec. 2013, Art. no. 1502431.
- [31] J. M. Dudley, G. Genty, and S. Coen, "Supercontinuum generation in photonic crystal fiber," *Rev. Mod. Phys.*, vol. 78, no. 4, pp. 1135–1184, Oct. 2006.
- [32] G. P. Agrawal, "Chapter 13 supercontinuum generation," in *Nonlinear Fiber Optics*, 5th ed. San Francisco, CA, USA: Academic, 2013, pp. 388–423.
- [33] J. H. Parker, D. W. Feldman, and M. Ashkin, "Raman scattering by silicon and germanium," *Phys. Rev.*, vol. 155, no. 3, pp. 712–714, Mar. 1967.
- [34] L. Carletti *et al.*, "Nonlinear optical response of low loss silicon germanium waveguides in the mid-infrared," *Opt. Express*, vol. 23, no. 7, pp. 8261–8271, Apr. 2015.
- [35] I. Pupeza *et al.*, "High-power sub-two-cycle mid-infrared pulses at 100 MHz repetition rate," *Nature Photon.*, vol. 9, pp. 721–724, Sep. 2015.
- [36] D. Seo, J. M. Gregory, L. C. Feldman, N. H. Tolk, and P. I. Cohen, "Multiphoton absorption in germanium using pulsed infrared free-electron laser radiation," *Phys. Rev. B*, vol. 83, no. 19, May 2011, Art. no. 195203.
- [37] B. Zhang *et al.*, "High brightness 2.2–12 μm mid-infrared supercontinuum generation in a nontoxic chalcogenide step-index fiber," *J. Amer. Ceram. Soc.*, vol. 99, no. 8, pp. 2565–2568, Jun. 2016.
- [38] F. Li, Q. Li, J. H. Yuan, and P. K. A. Wai, "Highly coherent supercontinuum generation with picosecond pulses by using self-similar compression," *Opt. Express*, vol. 22, no. 22, pp. 27339–27354, Nov. 2014.
- [39] G. Genty, M. Surakka, J. Turunen, and A. T. Friberg, "Complete characterization of supercontinuum coherence," *J. Opt. Soc. Amer. B*, vol. 28, no. 9, pp. 2301–2309, Sep. 2011.
- [40] R. Loo *et al.*, "High quality Ge virtual substrates on Si wafers with standard STI patterning," *J. Electrochem. Soc.*, vol. 157, no. 1, pp. H13–H21, 2010.
- [41] J. Chiles, S. Khan, J. C. Ma, and S. Fathpour, "High-contrast, all-silicon waveguiding platform for ultra-broadband mid-infrared photonics," *Appl. Phys. Lett.*, vol. 103, no. 15, Oct. 2013, Art. no. 151106.
- [42] A. Malik *et al.*, "Ge-on-Si and Ge-on-SOI thermo-optic phase shifters for the mid-infrared," *Opt. Express*, vol. 22, no. 23, pp. 28479–28488, Nov. 2014.

Jinhui Yuan received the B.S. and M.S. degrees from Yanshan University, Qinhuangdao, China, in 2005 and 2008, respectively. He received the Ph.D. degree from Beijing University of Posts and Telecommunications (BUPT), Beijing, China, in 2011.

He is currently with the BUPT as an Associate Professor. He is also a Hong Kong Scholar at the Photonics Research Centre, Department of Electronic and Information Engineering, The Hong Kong Polytechnic University. His current research interests include photonic crystal fibers, silicon waveguide, and optical fiber devices. He is a Member of OSA. He has published more than 100 papers in the academic journals and conferences.

Zhe Kang received the B.S. degree from Wuhan University of Technology, Wuhan, China, in 2006, the M.S. degree from Dalian Polytechnic University, Dalian, China, in 2012, and the Ph.D. degree from Beijing University of Posts and Telecommunications, Beijing, China, in 2015.

He is currently a postdoctoral fellow in The Hong Kong Polytechnic University. His research interests include ultrafast nonlinear optics and nonlinear silicon photonics.

Feng Li received the B.S. and Ph.D. degrees from University of Science and Technology of China, Hefei, China, in 2001 and 2006, respectively.

After that, he joined the Hong Kong Polytechnic University as a Postdoctoral Fellow. He is currently a Research Fellow at the Hong Kong Polytechnic University. His research interests include fiber lasers, especially multiwavelength lasers and mode locked lasers, nonlinear fiber optics, supercontinuum generation, and nonlinear dynamics in optical devices and optical systems.

Xianting Zhang received the B.S. and M.S. degrees from Beijing University of Posts and Telecommunications, Beijing, China, in 2013 and 2016, respectively. He is currently working toward the Ph.D. degree at The Hong Kong Polytechnic University.

His research interests include fiber lasers, optical signal processing, and nonlinear fiber optics.

Xinzhu Sang received the B.S. degree from Tianjin University, Tianjin, China, and the M.S. degree from Beijing Institute of Machinery, Beijing, China, in 1999 and 2002, respectively, and the Ph.D. degree from Beijing University of Posts and Telecommunications (BUPT), Beijing, China, in 2005. He is currently with the BUPT as a Professor.

From December 2003 to March 2005, he was with Optoelectronics Research Centre, Department of Electronic Engineering, City University of Hong Kong as a Research Assistant. From July 2007 to July 2008, he worked in University of California at Irvine as a Postdoctoral Research Scholar. His current research interests include novel photonic devices, optical communication, and optical interconnect. He is a senior member of Chinese Institute of Communication, a committee of Holography and Optical information Processing, Chinese Optical Society, and a member of OSA.

Qiang Wu received the B.S. and Ph.D. degrees from Beijing Normal University and Beijing University of Posts and Telecommunications, Beijing, China, in 1996 and 2004, respectively.

From 2004 to 2006, he worked as a Senior Research Associate in City University of Hong Kong. From 2006 to 2008, he took up a research associate post in Heriot-Watt University, Edinburgh, U.K. From 2008 to 2014, he worked as a Stokes Lecturer at Photonics Research Centre, Dublin Institute of Technology, Ireland. He is currently an Associate Professor at Northumbria University, U.K. His research interests include photonics devices and fiber optic sensing.

Binbin Yan received the B.S. and M.S. degrees from Beijing University of Posts and Telecommunications (BUPT), Beijing, China, in 2003 and 2005, respectively, and the Ph.D. degree in 2009 from the same university.

She is currently with the BUPT as a Lecturer. Her research interests include photonic devices and fiber optic sensing.

Kuiru Wang received the B.S. and M.S. degrees from Beijing University of Posts and Telecommunications (BUPT), Beijing, China, in 1984 and 1990, respectively. She received the Ph.D. degree from BUPT in 2009.

She is currently with the BUPT as a Professor. Her current research interests include optical fiber communication and photonic devices.

Xian Zhou received the Ph.D. degree in electromagnetic field and microwave technology from Beijing University of Posts and Telecommunications (BUPT), Beijing, China, in 2011. She is currently an Associate Professor at the Department of Computer and Communication Engineering, University of Science and Technology Beijing.

She is also a Hong Kong Scholar at the Photonics Research Centre, Department of Electronic and Information Engineering, The Hong Kong Polytechnic University. Her research interests are focused on high-speed optical communications, short reach communications, and digital signal processing.

Kangping Zhong was born in Jiangxi, China, in 1987. He is postdoctoral in Photonics Research Center at The Hong Kong Polytechnic University. He received the B.S. degree in electrical engineering from the Beijing Institute of Technology, Beijing, China, in 2008. He received the Ph.D. degree in communication and information engineering from Beijing Jiaotong University, Beijing, China, in June 2014. From 2011 to 2012, he was a Visiting Scholar in Lightwave System Research Laboratory at Queen's University in Kingston, Canada, supervised by Prof J. C. Cartledge working in the long haul coherent transmission systems.

From 2013, he was Research Associate and now is Postdoctoral Fellow in Photonics Research Center at The Hong Kong Polytechnic University. He has coauthored more than 20 papers in leading journals and conferences. His research interests include long haul coherent transmission systems, high-capacity IM/DD systems for optical interconnect and optical access networks and digital signal processing techniques for advanced modulation formats.

Guiyao Zhou received the B.S. degree from Jilin University, Jilin, China, in 1996, and received the M.S. and Ph.D. degrees from Yanshan University, Qinhuangdao, China, in 2003 and 2007, respectively.

He is currently a Professor at South China Normal University, Guangzhou, China. His current research interests include the photonic crystal fibers and optoelectronic devices.

Chongxiu Yu received the Graduate degree from the Beijing University of Posts and Telecommunications (BUPT), Beijing, China, in 1969. He is currently with the BUPT as a Professor. She is engaged in university education and research work and has been the Principal Investigator of many projects supported by China 863 plan, the National Natural Science Foundation and the National Ministry of Science Technology, etc. Up to now she has published more than 300 papers. Her research interests include the optical fiber communication, photonic switching, and optoelectronics technology and its applications.

Prof. Yu is a Member of Chinese Institute of Communication, Committee of Fiber Optics and Integral Optics, and Chinese Optical Society.

Chao Lu received the B.Eng. degree in electronic engineering from Tsinghua University, Beijing, China, in 1985, and the M.Sc. and Ph.D. degrees from the University of Manchester, Manchester, U.K., in 1987 and 1990, respectively. He joined the School of Electrical and Electronic Engineering, Nanyang Technological University, Singapore, in 1991 and served as a Lecturer, Senior Lecturer, and an Associate Professor until 2006. From June 2002 to December 2005, he was seconded to the Institute for Infocomm Research, Agency for Science, Technology and Research (A*STAR), Singapore, as the Program Director and Department Manager, helping to establish a research group in the area of optical communication and fiber devices. Since April 2006, he has been a Professor in the Department of Electronic and Information Engineering, the Hong Kong Polytechnic University. His research interests include optical communication systems and networks, fiber devices for optical communication and sensor systems.

Prof. Chao Lu is the Fellow of the Optical Society of America.

Hwa Yaw Tam (SM'09) received the B.S. and Ph.D. degrees from The University of Manchester, Manchester, U.K., in 1985 and 1990, respectively.

From 1989 to 1993, he was with Hirst Research Center, GEC-Marconi Ltd. in the U.K., first as a Research Scientist, then as a Senior Research Scientist working on WDM systems and fiber amplifiers. He also worked briefly for Marconi-Italiana of Italy as a Consultant before joining the Department of Electrical Engineering, Hong Kong Polytechnic in January 1993. He is currently the Chair Professor of Photonics with the Department of Electrical Engineering, The Hong Kong Polytechnic University, where he is also the Director of the Photonics Research Centre, Faculty of Engineering. His current research interests include silica and polymer fibre fabrication, FBGs and FBG-based transducers, fiber amplifiers, optical communication systems, and all-optical signal processing. He has authored or coauthored about 400 papers and holds eight patents in the areas of fiber optics.

Prof. Hwa Yaw Tam is a fellow of the Optical Society of America.

P. K. A. Wai (SM'96) received the B.S. (Hons.) degree from the University of Hong Kong, Pok Fu Lam, Hong Kong, in 1981, and the M.S. and Ph.D. degrees from the University of Maryland, College Park, MD, USA, in 1985 and 1988, respectively.

In 1988, he joined Science Applications International Corporation, McLean, VA, USA, where he was a Research Scientist involved with the Tethered Satellite System Project. In 1990, he became a Research Associate with the Department of Physics, University of Maryland, College Park, and the Department of Electrical Engineering, University of Maryland, Baltimore County. In 1996, he joined the Department of Electronic and Information Engineering, The Hong Kong Polytechnic University. He became the Chair Professor of Optical Communications in 2005. He is currently the Vice-President (Research Development). His research interests include soliton, fiber lasers, modeling and simulations of optical devices, long-haul optical fiber communications, all-optical packet switching, and network theories. He is an active contributor to the field of photonics and optical communications, having authored or coauthored more than 300 international refereed publications. He is currently an Associate Editor of the *Journal of Lightwave Technology*.

Prof. P. K. A. Wai is the fellows of the IEEE and OSA.

